Drone Systems and Applications

OPEN ACCESS I Article

Optical reflectance across spatial scales—an intercomparison of transect-based hyperspectral, drone, and satellite reflectance data for dry season rangeland

Glenn SladeCP, Dominic Fawcett(EP, Andrew M. Cunliffe CP. Richard E. Brazier (Y, Kamal Nyaupane of Marguerite Mauritz Sergio Vargas (Db, and Karen Anderson Od

al)epartment of Geography, Faculty of Environment, Science and Economy, University of Exeter, Exeter, UK; bEnvironmental Science and Engineering Program, The University of Texas at El Paso, 500 W University Avenue, El Paso, TX 79968, USA; ^C Biological Sciences, o The University of Texas at El Paso, 500 W University Avenue, El Paso, TX 79968, USA; dEnvironment and Sustainability Institute, University of Exeter, Penryn Campus, Exeter TR109FE, UK

Corresponding author: Glenn Slade (email: gs558@exeter.ac.uk)

Abstract

Drone-based multispectral sensing is a valuable tool for dryland spatial ecology, yet there has been limited investigation of the reproducibility of measurements from drone-mounted multispectral camera array systems or the intercomparison between drone-derived measurements, field spectroscopy, and satellite data. Using radiometrically calibrated data from two multispectral drone sensors (MicaSense RedEdge (MRE) and Parrot Sequoia (PS)) co-located with a transect of hyperspectral measurements (tramway) in the Chihuahuan desert (New Mexico, USA), we found a high degree of correspondence within individual drone data sets, but that reflectance measurements and vegetation indices varied between field, drone, and satellite sensors. In comparison to field spectra, MRE had a negative bias, while PS had a positive bias. In comparison to Sentinel2, PS showed the best agreement, while MRE had a negative bias for all bands. A variogram analysis of NDVI showed that ecological pattern information was lost at grains coarser than 1.8 m, indicating that drone-based multispectral sensors provide information at an appropriate spatial grain to capture the heterogeneity and spectral variability of this dryland ecosystem in a dry season state. Investigators using similar workflows should understand the need to account for biases between sensors. Modelling spatial and spectral upscaling between drone and satellite data remains an important research priority.

Key words: drone, multispectral, Parrot Sequoia, MicaSense RedEdge, Sentinel-2, dryland

1. Introduction

A third of the world's population is estimated to live in drylands, which cover approximately 41% of the Earth's land surface (Safriel and Adeel 2005). Drylands are predicted to increase in global extent to cover 50% of the land by 2100 (Nagler et al. 2007). Climate change is also predicted to shift ecosystem mechanisms currently prevalent in drylands into historically wetter climatic zones (Grünzweig et al. RS products (e.g., MODIS17A2) demonstrate poor

ing ecosystem-level information on dryland parameters satellite remote sensing (RS) data remains a challenge due to scaling issues related to the heterogeneous nature of dryland ecology (Biederman et al. 2017; Fawcett et al. 2022), low vegetation signal-to-noise ratios relative to bright soil backgrounds, and high dynamism in relation to seasonal rainfall variability (Smith et al. 2019). Furthermore, some satellite correspon2022). Dryland climates have a high degree of temporal rain- dence with temporal patterns of gross ecosystem fall variability (Schlesinger et al. 2009; Thomey et al. 2011) and, as water-limited ecosystems, C uptake and release are sensitive to this variability, leading to variations in aboveground biomass (AGB) (Houghton et al. 2001; McDowell et al. 2008; Vargas et al. 2012). Increasingly, this variability of dryland ecosystems is being recognised as important in the context of the global C cycle (Poulter et al. 2014; Ahlström et al. 2015; Sitch et al. 2015). For this reason, it is important that robust methodologies are developed for monitoring dryland vegetation conditions and dynamics over space and time, and yet, various studies have shown that retriev-

and geomorphologists because research has shown that factors such as vegetation patterns and connectivity are fundamental to understanding dryland productivity and the provision of ecosystem services (Schlesinger and Pilmanis 1998; Schlesinger et al. 2009', Mayor et al. 2013; Okin et al. 2015).

While the relatively coarse grain of satellite observations makes retrieval of dryland surface properties challenging, there are alternative approaches that can be used proximally to deliver useful scale-appropriate information about dryland dynamics, and these have been widely tested. Within plant sciences, drone methodologies have progressed significantly over the past decade, with great potential to deliver information about plant community assemblages and structural ecosystem parameters (Assmann et al. 2020; Sun et al. 2021). Indeed, dryland scientists have experimented with drone-captured imaging data for describing ecosystem vario

u ability (examples include Laliberte et al. 2011; Swetnam et al. 2018; Sankey et al. 2019). Photogrammetric workflows applied to drone data in drylands have delivered unique insights into spatial ecology, plant structural forms, and biomass distribution (Cunliffe et al. 2016, 2022a; McIntire et al. 2022). Closer to the ground, Gamon et al. (2006a) have demonstrated the rich information content of hyperspectral information from transects sampled by automated tramways in Californian chaparral. While there have been some experiments outside of drylands that have successfully undertaken scaling of data between drone-based and satellite observations (e.g., Fernandez-Guisuraga et al. 2018; Franzini et al. 2019; Assmann et al. 2020; Fawcett et al. 2020; Lu et al. 2020), less attention has been given to this challenge in drylands despite the potentially important ramifications of combining data across these

productivity measured at the site level by flux tower observations, capturing less than 30% of the observed interannual variability (Biederman et al. 2017). There is a bias in remote sensing studies of dryland ecosystems towards sampling at peak greenness, with a lack of corresponding studies undertaken in dry season conditions. The latter is critical for monitoring seasonal fluctuations in C, but patterns and dynamics much less well understood, with little information on how products at different scales might perform under these conditions. Crucially, the spatial and temporal heterogeneity of dryland ecosystems is relevant for ecologists, soil scientists,

scales of measurement (from spatial spectroscopy to drones and then to satellite observations). There is a strong argument for undertaking multiscale experiments in drylands to address the "scale mismatch" between remote sensing and other observations of carbon stocks and fluxes (Gamon 2015) and to support the appropriate scaling of field-based physiology measurements and the individual plant or eddy covariance footprint level to larger landscape 0 or regional scales (Cunliffe et al. 2022b).

> This study builds on the vision proposed in Gamon et al.'s (2006b) Spectral Network paper, which (SPECNET) advocates for experiments that compare optically sampled datasets across different scales. We address the key knowledge gaps in how optical remote sensing datasets at different scales compare with each other in dry season (low biomass) conditions. We use a position transect fixed of hyperspectral measurements sampled by a tramway system equipped with a hyperspectral sensor at the Jornada Basin Experimental Range in New Mexico, USA. Concurrently with the hyperspectral measurements along the transect, multispectral data were acquired from two drone multiple camera array sensors (Parrot Sequoia (PS) and MicaSense RedEdge-M (MRE)). These two systems were compared because previous work has shown radiometric accuracy and consistency with such minicamera. array-based imaging radiometers to be quite variable (Franzini et al. 2019; Fawcett et al. 2020; Lu et al. 2020; Olsson et al. 2021). Our goal was to

Fig.

examine the relationship between the hyperspectral data near the ground and products delivered from the dronecaptured data before comparing it with satellite data captured by Sentinel-2. We address the following research questions for a dryland ecosystem in dry season conditions:

- 1. What is the correspondence within and between datasets captured by MRE and PS sensors?
- 2. What is the relationship between data captured from lightweight multispectral sensors on drones and field spectroradiometric measurements?
- 3. What is the spatial grain of semivariance in NDVI?
- 4. To what extent do vegetation indices correspond between drone-captured and Sentinel-2 image data in drylands?

2. Materials and methods

2.1. Study site

The study was conducted on a site with open shrubland vegetation cover in the northern Chihuahuan Desert, New Mexico, USA, which is described in more detail by Monger et al. (2006) and Rango et al. (2006). The study site was on a piedmont slope (bajada) of the San Andreas mountains, located within the Jornada Basin Experimental Range (latitude 32.582, longitude —106.635). The site lies at ca. 1188 m above mean sea level, with a mean annual temperature of 14.7 °c and a mean annual precipitation of 245 mm. The dominant shrubs are evergreen Larrea tridentata (creosote

bush) and winter-deciduous Prosopis glandulosa (honey mesquite). Other cover types at lower density include Flourensia cernua (tarbush) and patchy occurrences of the grasses Muhlenbergia porteri (bush muhly) and Dasyochloa pulchella (fluff grass). Prosopis glandulosa and F. cernua were both in a leaf-off state at the time of the survey. The site occasionally experiences grazing and browsing by stray domestic cattle, free-ranging introduced Oryx, and native mammals (jack rabbits and desert pronghorn). The soils at the site are Ustic Calciargids, and the underlying parent material consists of limestone, other sedimentary rock, and some igneous rock. The study site is adjacent to the US-JOI flux monitoring station, which produces high-frequency measurements of energy, water, and C0² flux.

2.2. Overall experimental design

The experiment was designed to capture multiple drone surveys with the PS and MRE sensors coincident with hyperspectral measurements of surface reflectance sampled at fixed positions along a transect. Figure la shows the location of the site. Detailed experimental aspects are described in subsequent sections.

Figure 2 provides an overview of the timing of data capture, where field measurements and drone surveys were captured entirely on 24 February 2020, and the Sentinel-2 overpass occurred on the previous day. Three sets of drone surveys were flown over the tramway area of interest (AOI) and one set over a wider AOI, with the tramway measurements taken on three passes at the start, middle, and end of the drone survey period (Fig. 2).

1. Location of the study site (a), photograph of tramway spectrometer in operation (b), location map of the tramway position (red line), tramway area of interest (AOI) for drone surveys (green rectangle), and area AOI for wider drone surveys (c); taking pre-flight calibration reference images, separate calibration images were taken centred over each panel in turn, hence why some panels here are shown as shaded since they are not being measured (d), and diagram of tramway measurement footprints superimposed on a true colour orthomosaic of part of the tramway (e).

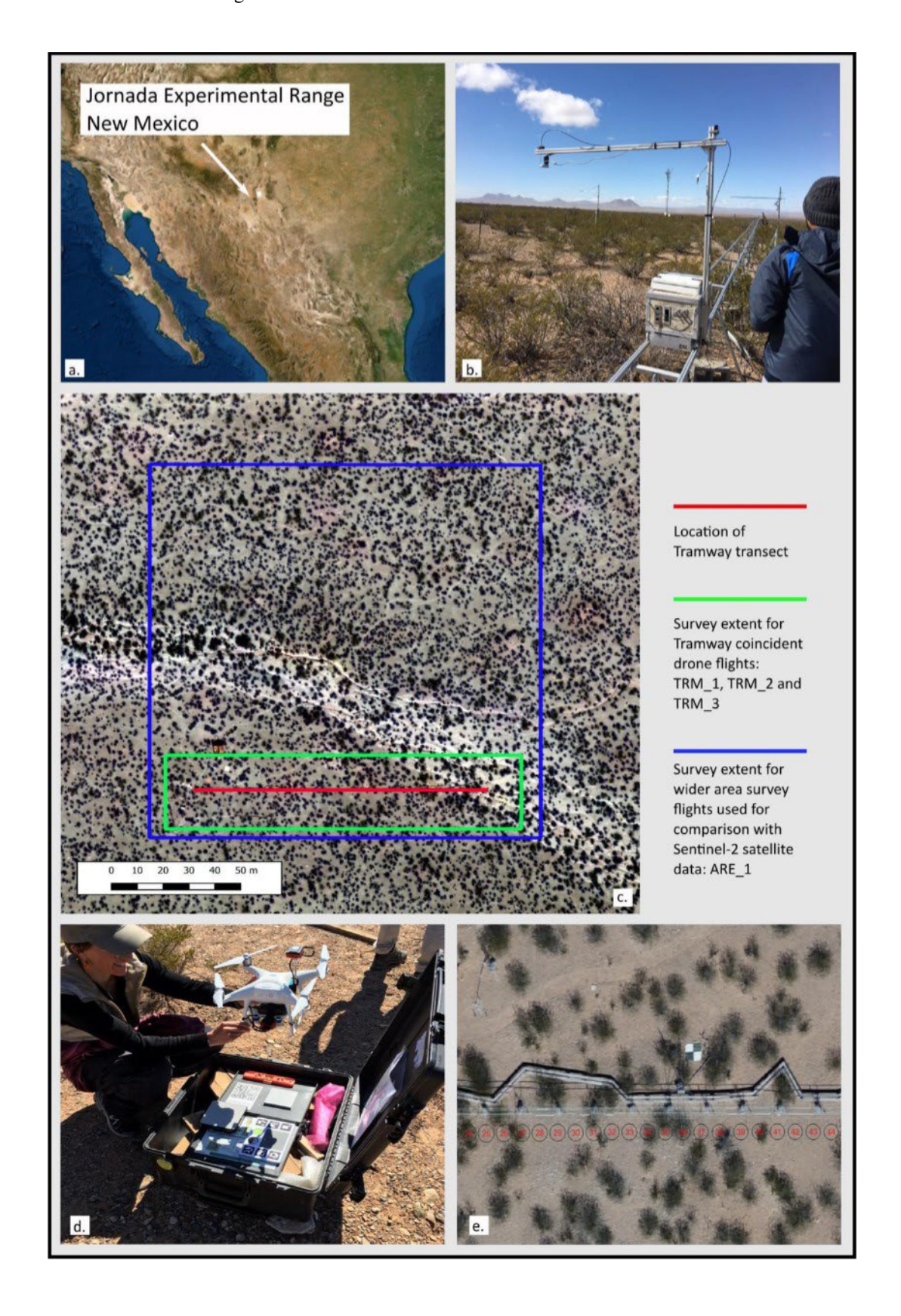
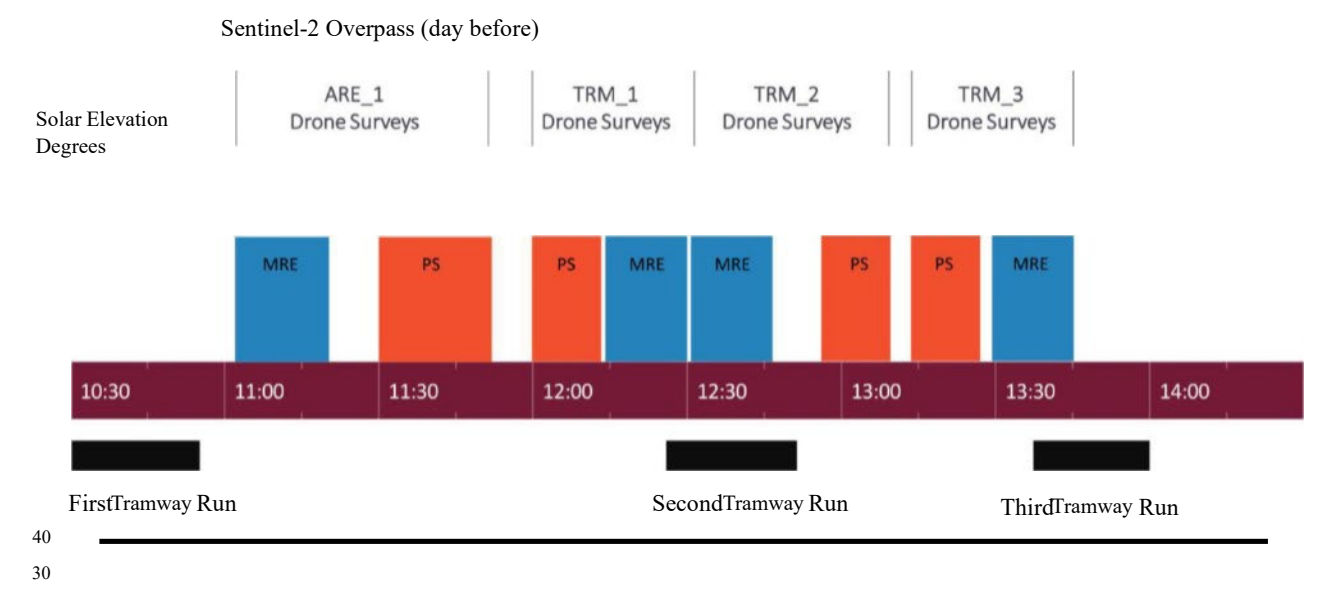


Fig.

2. Schematic illustration of the timing of data acquisition relative to solar elevation—all field data were captured on 24 February 2020, while the Sentinel-2 scene was captured on 23 February 2020. The time stated is local time (UTC -7). MRE— MicaSense Red Edge sensor. PS—Parrot Sequoia sensor. ARE_1—Larger area drone survey shown in Fig. lc. TRM I, 2, and 3—tramway-focused drone survey shown in Fig. IC.



2.3. Atmospheric conditions during data acquisition

All drone survey flights on 24 February 2020 were conducted in cloud-free (Sky code O after Assmann et al. 2018) sunny conditions with a wind speed less than 4 mls. The mean air temperature on the survey day was 9 ° c with a maximum of 18 ° c, minimum of 0.4 °c and no precipitation recorded. On the 23 FebruaIY (Sentinel-2 overpass), the mean air temperature was Il ° c, the maximum was 14 °c, the minimum was 4 °c, and 0.2 mm of total precipitation was recorded for the 24 h period.

2.4. Tramway field hyperspectral measurements

The ground remote sensing platform is a robotic tram system, equipped with a cart hosting a dual detector spectrometer at the Jornada Experimental Range (JER) to monitor ecosystem optical properties. The tramline (pictured in Fig. 1b) is 110 m long and was installed with the intent to sample the dominant species present (e.g., P. glandulosa (honey mesquite), Larrea tridentate (creosote), and bare ground (shrub interspace)). The tram system is similar to that described by Gamon et al. (2006a) for a California Chaparral ecosystem and forms part of a larger Long Term Ecological Research (LTER) study (Havstad et al. 2020). The instrument used in the cart is a dual detector spectrometer (Unispec DC; PP System, Amesbury, MA, USA) that contains two detector channels, one for radiance from the target and the other for downwelling irradiance. The spectral range for this instrument is from 310 nm to approximately 1130 nm with a 3 nm resolution. The

spectrometer was triggered by metal markers situated every meter on the tramline, with measurements acquired on three runs at separate times, as outlined in Fig. 2.

For the final reflectance calculation, the ratio between radiance and irradiance was corrected using a reference calibration of a 99% reflective white standard panel. The collected spectral reflectance was processed using rHyperSpec software (https://lseI-jornada.shinyapps.iolrHyperSpecl) (Laney 2013) to extract the hemispherical conical reflectance factor (HCRF) reflectance that we used in this study for further analysis.

2.5. UAV image data and processing

Twomultispectral multi-camera array sensors were used in the study. Their spectral response curves are given in Fig. 3 relative to those from the corresponding Sentinel-2 bands. We flew three surveys concentrating on the tramway AOI (130 m x 20 m) and one survey over a wider area (covering 130 m x 200 m) as detailed in Table S2. All survey flights were conducted in cloud-free (Sky code O after Assmann et al. 2018) sunny conditions with a wind speed less than 4 mls and an air temperature of ca. 14—18 °c. The locationlextent of the tramway-focused surveys (TRM_I, TRM_2, and TRM 3) and wider area surveys (ARE 1) are shown in Fig. lc.

0

0

0

6

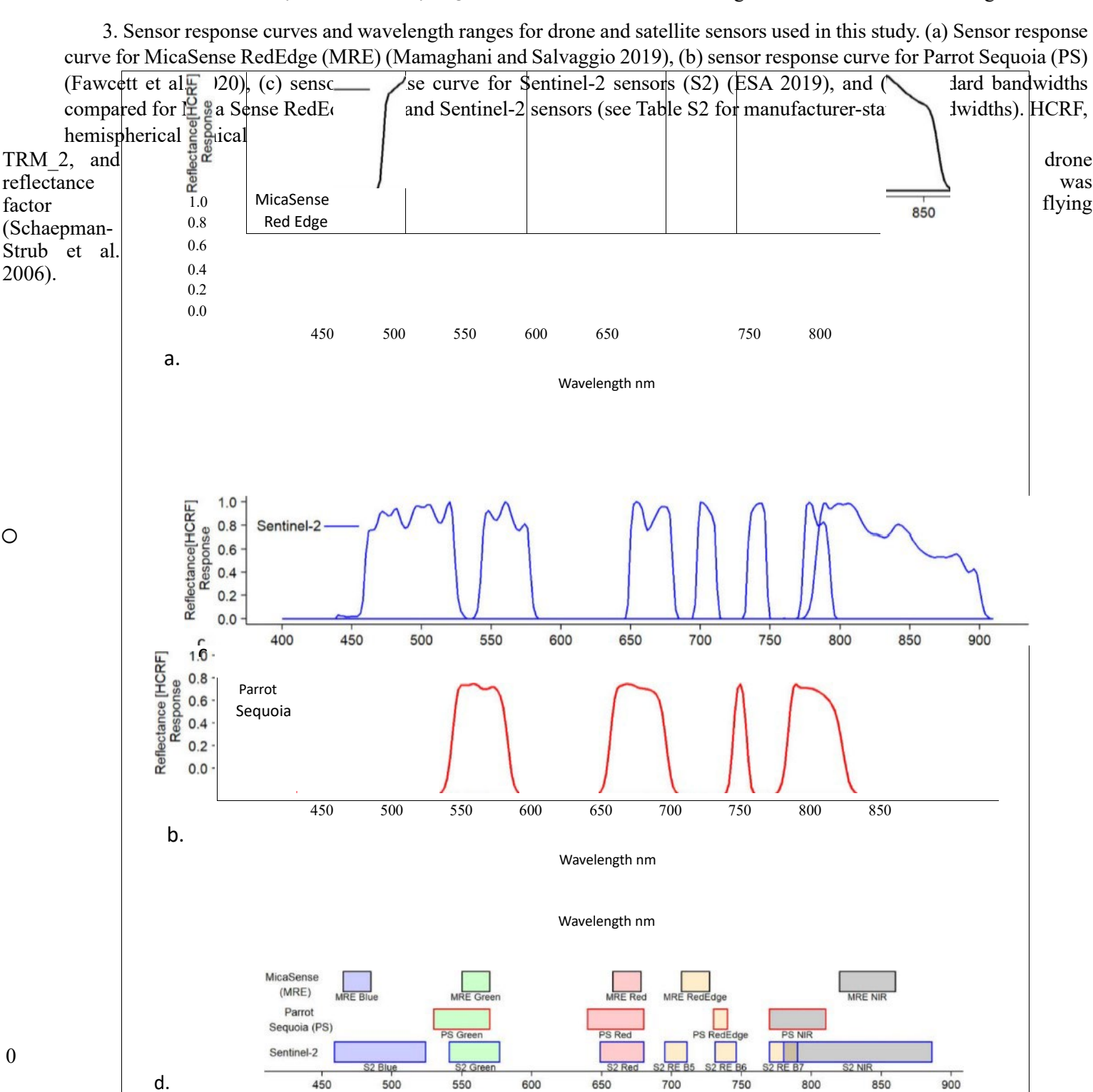
2.5.1. Parrot Sequoia image data

Drone image data were acquired using a PS multi-camera array attached to a 3-D-printed mount on a DJI Phantom 4 Advanced multirotor UAV. The sensor was angled by ca. 10 degrees to attain a near-nadir angle when the drone was flying forward. The Sequoia measures light in the green, red, red edge, and NIR wavelength regions, as detailed in Table Sl. The PS survey flight height of 50 m (Table S2) resulted in a ground sampling distance (GSD) of 5.08, 5.29, and 5.36 cm for the tramway-focused survey flights TRM 1, TRM 3, respectively. The larger survey area (ARE 1) was flown at a height of 67 m, resulting in a GSD of 6.63 cm.

2.5.2. MicaSense RedEdge-M data

Drone image data were acquired using a MRE-M multicamera array mounted on a DJI Phantom 4 Pro Platinum multirotor UAV. The sensor was angled by ca. 10 degrees to attain a near-nadir angle when the

dx.doi.orq/10.1139/dsa-2023-0003



Drone syst. App. 11: 1-27 (2023)

Fig.

forward. The MRE sensors record light in the blue, green, red, red edge, and NIR wavelength regions as detailed in Table Sl. The MRE spatial sensor resolution is finer than the PS sensor, and flight heights of 80 m and 110 m (Table S2) were implemented to achieve similar GSD for both sensor surveys. GSD was 5.33, 5.46, and 5.43 cm for the tramwayfocused MRE survey flights and 7.42 cm for the larger ARE I survey area.

2.5.3. Processing of drone data

The image data from each of the PS and MRE drone surveys were processed in Pix4D software version 4.8.0 (Pix4D, Switzerland), including geometric correction using at least five precisely geolocated ground control points and radiometric calibration to surface reflection (Assmann et al. 2018).

> Radiometric calibration was performed using preflight images of a SpectralonTM grey reference target with 43% average reflectance over the PS wavelength range. This was used instead of a white reference panel to avoid saturation. A subset of the original survey set was used to produce an orthomosaic of surface reflectance for each band for the tramway area, using only flight lines closest to nadir above the tramway to avoid any images with a lower angle of observation being used within the reconstruction of the orthomosaic for the tramway footprints.

2.6. Sentinel-2 image data

A Sentinel-2 A bottom of atmosphere (L2A) reflectance image for the closest available date to the field and drone data acquisition, 23 February 202010:43 local time (the day before drone flights and spectral tramway data capture; Fig. 2), was downloaded from the ESA Copernicus Open Access Hub. The meteorological conditions were similar on the satellite image data acquisition date/time to the drone and tramway surveys. The image bands used for this study were blue (B2—IO m spatial resolution), green (B3—IO m spatial resolution), red (B4—10 m spatial resolution), red edge (B5, 136, and B7—20 m spatial resolution), and NIR (B8-IO m spatial resolution), with band wavelength regions given in Table SI. The sensor response curve for Sentinel-2 is given in Fig. 3, with comparisons with the manufacturersupplied band wavelength regions for the PS and MRE multiple camera arrays.

Multitemporal co-registration of Sentinel-2 image data is known to be of the order of one pixel or 12 m accuracy (Rufin et al. 2021). To facilitate the direct comparison of the drone-acquired image data and Sentinel-2 image data, the coregistration between drone and satellite data was checked by spatially resampling the drone data to the coarser 10 m resolution of the Sentinel-2 image data and visually comparing the images. We checked co-registration using the co-register Images function in R (RStoolbox

package version 0.3.0) and found that the georegistration as supplied by ESA was opti-

2.7. Planetscope fine spatial resolution satellite image data

A PlanetScope scene image from the Dove-R instrument (instrument id PS2.SD) for 24 February 2020, 10:49 local time (the same day as the tramway and drone data acquisition) was ordered and downloaded from the Planet Explorer website. The PlanetScope image data has a 3 m pixel resolution comprising blue, green, red, and near-infrared bands and was used within this study to facilitate a spatial comparison of data at an intermediate spatial resolution between the drone and Sentinel-2 image data. Due to the unavailability of sensor response functions, the PlanetScope image data were not included in the spectral intercomparison with drone and hyperspectral data.

2.8. Intercomparison of data from tramway hyperspectral instrument and drone sensors

To facilitate comparison of multiscale sensors, the drone data were resampled to the spatial resolution of the tramway measurement footprints using the methodolow described below. The footprint of each hyperspectral measurement was delineated as a polygon using a projected field-of-view based on survey-grade GNSS observations combined with a digital surface model. These polygons were used in R (R Core Team 2021) to extract surface reflectance from the drone image data and produce an average reflectance value for each tramway measurement location for each sensor band using the "exact extract" function (exact extractr package, version 0.9.1) (Baston and ISciences 2022). Due to the varying height of the tramway along its length, these footprints varied from 0.67 to 1.06 m in diameter, which sampled between 154 and 385 drone image pixels per footprint (at a GSD of 5.4 cm). In addition to comparing individual drone survey data for each footprint, the three drone survey observations were averaged (using the mean) to streamline the comparison between hyperspectral and drone sensor measurements.

facilitate intercomparison the of spectral measurements, tramway-derived hyperspectral reflectance values were spectrally resampled using the sensor response functions for the PS (D'Odorico et al. 2013) and MRE-M (Mamaghani and Salvaggio 2019) following the method010U described by D'Odorico et al. (2013) to produce HCRF datasets spectrally comparable to the respective drone sensors (Fig. 3). Comparisons between

Canadian Science Publishing

data sets were performed in R, with assessments made using the mean absolute deviation (MAD). To evaluate the agreement between variables, we calculated Lin's concordance correlation coefficient (CCC) (Lin 1989, 2000) using the DescTools package (Signorell Andri et Multi 2022). We used strength of agreement interpretations of the CCC following criteria suggested by McBride (2005), where CCC values of >0.99 are described as almost perfect agreement, values between 0.95 and 0.99 are described as substantial agreement, values between 0.90 and 0.95 are described as moderate agreement, and values below 0.90 are described as poor agreement. We used total least squares regression to fit linear models that account for uncertainty in both dependent and independent variables. Formulae for the vegetation indices Normalised Difference Vegetation Index (NDVI), Soil Adjusted Vegetation Index (SAVI), Modified Soil Adjusted Vegetation Index (MSAV12), and Modified Triangular Vegetation Index (MTV12) used in this study are given in Table S3.

2.9. Intercomparison of drone and satellite data

To enable spatially explicit comparison of PS and MRE with the Sentinel-2 data, the drone data were processed by extracting mean data using a shapefile generated from the 10 m Sentinel-2 grid resolution using the exact extractr package in R.

To assess the spatial grain of semivariance of spectral reflectance in both the PS and MRE image data, we randomly sampled the data to 25% of image pixels, applied the vari-

Table 1. Summary statistics for the intercomparison of reflectance measurements derived from the three Parrot Sequoia (PS) surveys.

PS surveys-intercomparison of reflectance measurements

		Sensor Band					
	Survey results						
_	TRMI compared with TRM2	Green	0.004	0.984	0.991		
			0.006	0.984	0.992		
		Red edge	0.007	0.975	0.987		
		Near-infrared	0.008	0.976	0.986		
-	TRM2 compared with TRM3	Green	0.003	0.989	0.994		
			0.005	0.990	0.994		
		Red edge	0.007	0.980	0.990		
		Near-infrared	0.006	0.987	0.992		
-	TRMI compared with TRM3	Green	0.006	0.951	0.974		
			0.010	0.952	0.976		
ote: Mean absolute deviation		Red edge	0.012	0.934	0.966		
(MAD), coefficient of etermination (R2), and Lin's concordance correlation-		Near-infrared	0.013	0.934	0.961		

are values presented.

ogram function, and fitted models using the "gstat" package in R (Pebesma 2004; Gräler et al. 2016). The image sampling was required to achieve a reduction in data size sufficient to run the variogram function on the workstation available.

To derive a map of vegetation cover for the study area, a random forest classification of the MRE drone image data (survey ARE I) was carried out in Python using the Scikitlearn machine learning package (Pedregosa et al. 2011). Training polygons for two classes, vegetation cover (all types) and bare ground, were manually digitised by one operator directly onto the MRE drone image orthomosaic and randomly split into training (100 polygons) and validation (50 polygons) data sets. A six-layer image stack containing NDVI and the five reflectance bands was used in the random forest machine learning process to produce a binary classification of vegetation cover. Grid vector files matching the 10 m resolution Sentinel-2 pixel resolution and 3 m resolution PlanetScope (L3B) pixels were developed in R. The fractional vegetation cover (WC) for each grid pixel was calculated from the veg, etation cover classification image using the zonal statistics package in QGIS (QGIS Development Team 2009).

3. Results

3.1. Reproducibility of drone image data from different survey flights

Intercomparison plots between individual survey flights for the PS and MRE sensors of data extracted for each tramway footprint are presented in Figs. Sl, S2, S3, S4, and S5, with summary statistics presented in Tables 1 and 2 The PS sensor data extracted from the three coefficient (CCC)

survey flights TRMI, TRM2, and TRM3 had low variation betw^meen survey flight reflectance measurements, with a MAD of betw^meen 0.003 and 0.013 across all sensor bands (Table 1). The agreement between PS survey reflectance measurements was substantial to almost perfect, with Lin's CCC between 0.961 and 0.994. Similarly, the MRE survey measurements had substantial agreement between surveys (Table 2). with a CCC of between 0.963 and 0.996 and a MAD of between 0.011 and 0.002. The intrasensor agreement between the three surveys for the PS and MRE sensors justified the use of mean values from the three surveys in the remaining analysis presented in this paper.

3.2. Comparison of PS and MRE reflectance measurements

Intercomparisons between PS and MRE surface reflectance measurements extracted for tramway footprints are shown in Fig. 4. For all sensor bands, the PS recorded higher reflectance values than the MRE, with moderate agreement for the NIR and green bands (CCC 0.934 and 0.907, respectively) and poor agreement for the red and especially the red edge bands (CCC 0.842 and 0.642, respectively) (interpretations after McBride (2005)). A higher calculated NDVI resulted for MRE data compared with the PS (Fig. 5), with a CCC value of 0.621. It should be noted that the centre wavelengths and bandwidth of the sensor bands in the electromagnetic spectrum differ between the camera systems (Fig. 3 and Table SI), and to explore this further, we resampled the hyperspectral tramway data for both PS and MRE bandwidths and then calculated and plotted the resulting NDVI (Fig. S6). This analysis shows that the MRE sensor bandwidth locations result in higher NDVI values; however, the difference in NDVI that can be attributed to the sensor positions is smaller (NIAD: 0.011, CCC: 0.983)

compared with the difference in survey results (MAD: 0.07, CCC: 0.619) between the two sensors.

3.3. Comparison between tramway hyperspectral field spectral measurements and dronederived sulface reflectance

Intercomparison plots of tramway hyperspectral measurements and drone survey derived surface reflectance (mean data) measurements are presented in Fig. 6 for blue, green,

The MRE multiple camera array (MCA) sensors recorded slightly lower reflectance in blue, green, red, and red edge bandwidths compared with hyperspectral measurements, with CCC agreement values of 0.842, 0.836, 0.92, and 0.924, respectively (Table 3 and Fig. 6). Reflectance measurements for the NIR band showed a slightly positive bias (CCC: 0.891) compared with hyperspectral measurements, with the fitted slope indicating that this bias reduces with higher reflectance values. NDVI calculated from the MRE image data has

Table 2. Summary statistics for the intercomparison of reflectance measurements derived from the three MicaSense RedEdge (MRE) surveys.

	MRE surveys intercomparison of reflectance measurements				
-	Survey results	Sensor band	R2		
-	TRMI compared with TRM2	Blue	0.002	0.993	0.994
		Green	0.002	0.994	0.996
			0.004	0.993	0.996
		Red edge	0.003	0.991	0.996
		Near-infrared	0.004	0.988	0.994
-	TRM2 compared with TRM3	Blue	0.005	0.981	0.971
		Green	0.005	0.972	0.977
			0.008	0.978	0.984
		Red edge	0.009	0.973	0.977
		Near-infrared	0.006	0.972	0.982
-	TRMI compared with TRM3	Blue	0.004	0.957	0.969
		Green	0.006	0.956	0.973
			0.010	0.958	0.970
e: Mean absolute deviation (MAD),		Red edge	0.011	0.949	0.963
pefficient of determination (R ²), and Lin's concordance correlation—		Near-infrared	0.009	0.936	0.963

coefficient (CCC) values are presented.

red, red edge, and NIR wavelength bands, and summary statistics for the intercomparison are presented in Table 3. Plots of the individual drone survey data compared with corresponding tramway measurements are presented in Figs. S7, S8, S9, SIO, Sli, S12, S13, and S14. NDVI derived from hyperspectral tramway measurements is compared with drone data in Fig. 7.

The PS sensor data had a positive bias in the red, red edge, and NIR bands compared with the hyperspectral instrument, with poor CCC agreement values of 0.846, 0.732, and 0.803, respectively (Table 3 and Fig. 6). There was a closer agreement in the PS green wavelength band, with a moderate agreement

CCC of 0.921. NDVI values derived from the PS did not have a 1: 1 relationship with hyperspectral field measurements, with 0 the fitted linear model indicating that NDVI values tend to be positively biased for values below 0.15 and negatively biased for higher NDVI values, as shown in Fig.

a positive bias with a constant higher offset compared with tramway measurements (CCC: 0.677). MREderived NDVI had a higher difference with hyperspectral data than with PS data (Fig. 7). The statistical measures presented in Table 3 would appear to suggest that with better agreement in the red and NIR wavelengths, the MRE sensor should also be closer in NDVI to the hyperspectral data; however, the MAD and CCC values do not reflect the relative positive and negative bias in these bands that results in a larger difference in NDVI.

3.4. Comparison between vegetation indices derived from hyperspectral field and drone measurements.

We tested the correspondence across several different vegetation indices widely used in studies of dryland ecosystems. Comparison plots of vegetation indices (NDVI, SAVI, MSAV12, and M^EIV12) for MRE and PS image data

 \supset

Fig.

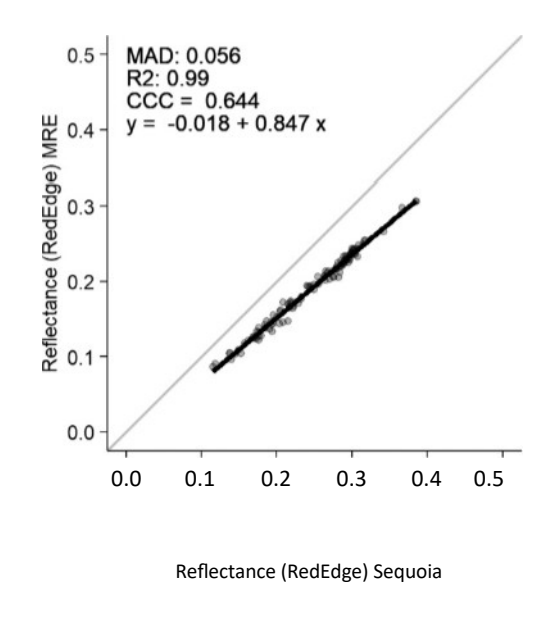
0

compared with tramway data are shown in Figs. S15 and S16, respectively, with summary statistics given in Table 4.

For MRE image data, the SAVI, MSAV12, and MTV12 calculated vegetation indices have less variation (MAD: 0.036, 0.032, and 0.016, respectively) than NDVI (MAD: 0.061) and demonstrate a smaller positive bias than NDVI. Only the MIVI calculated values for MRE data have a higher agreement (CCC: 0.843) than the NDVI (CCC: 0.679) with those calculated from tramway measurements.

For PS-derived vegetation indices, the SAVI, MSAV12, and MTV12 all have less variation in values compared with hyperspectral tramway measurements (MAD: 0.012, 0.011, and 0.017, respectively) than the NDVI (MAD: 0.024) and less variation compared with MRE-derived equivalent vegetation indices. SAVI, MSAV12, and MIVI indices all had lower agreementwith the hyperspectral tramway data (CCC: 0.858, 0.846, and 0.82, respectively) than NDVI (CCC: 0.868).

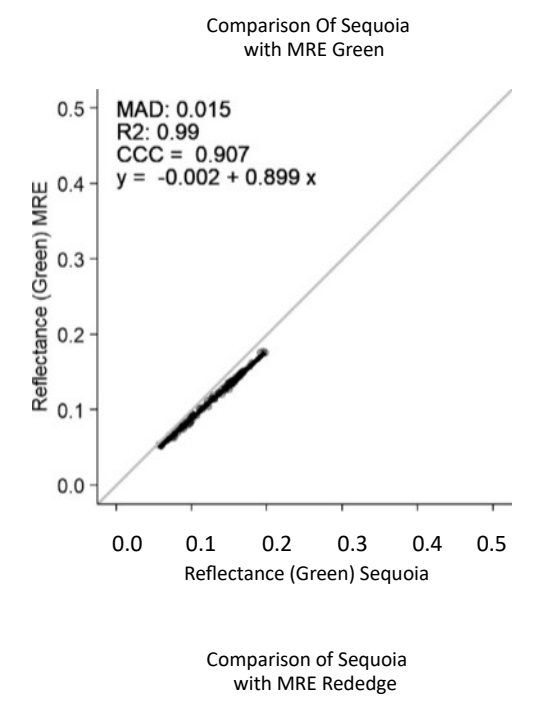
Broadly, the data show that adopting alternative vegetation indices to NDVI in the comparison with tramway data reduces the variability in the data but does not improve the agreement as measured by Lin's CCC except for the NfIV12 used with MRE data.

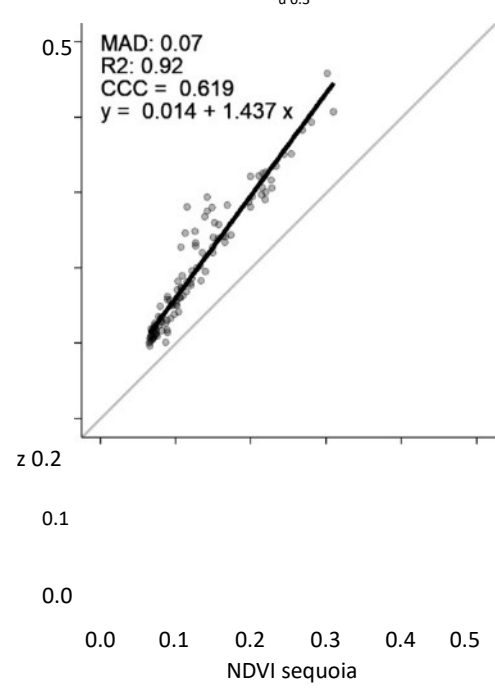


Comparison Of Sequoia with MRE NOVI

4. Comparison of Parrot Sequoia (Sequoia) and MicaSense RedEdge (MRE) reflectance for green, re nearinfared (NIR) sensor bands, and NDVI for all survey data (mean for each tramway footprint). Th $\epsilon^{0.4}$ deviation (MAD), coefficient of determination (R²), and Lin's concordance correlation coefficient (presented.

0





Syst. 11.•

Drone Appl. 1-27 (2023) dx.doi.org/10.1139/dsa-2023-0003 11

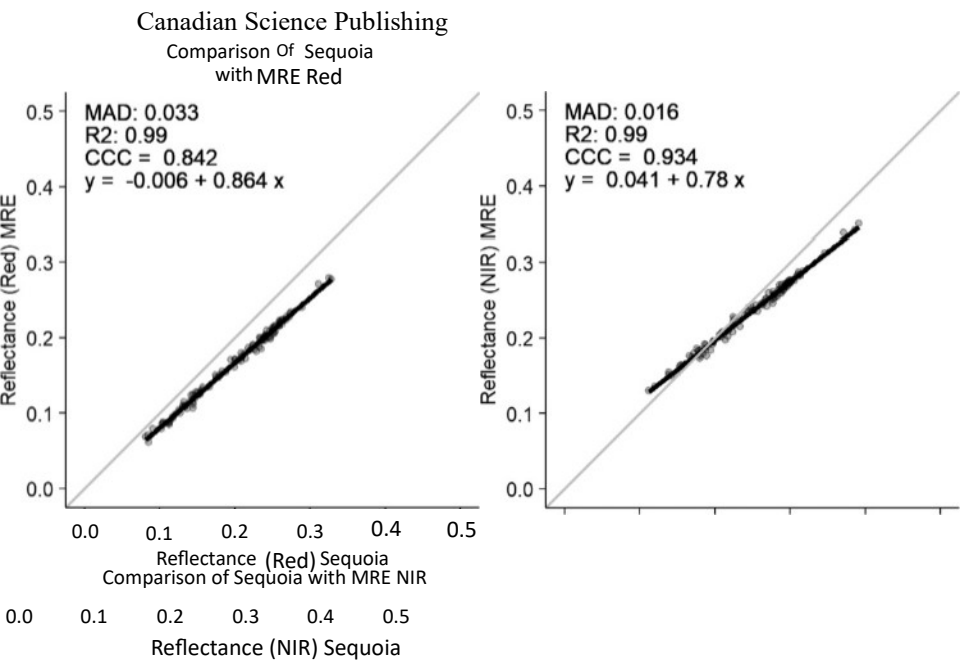
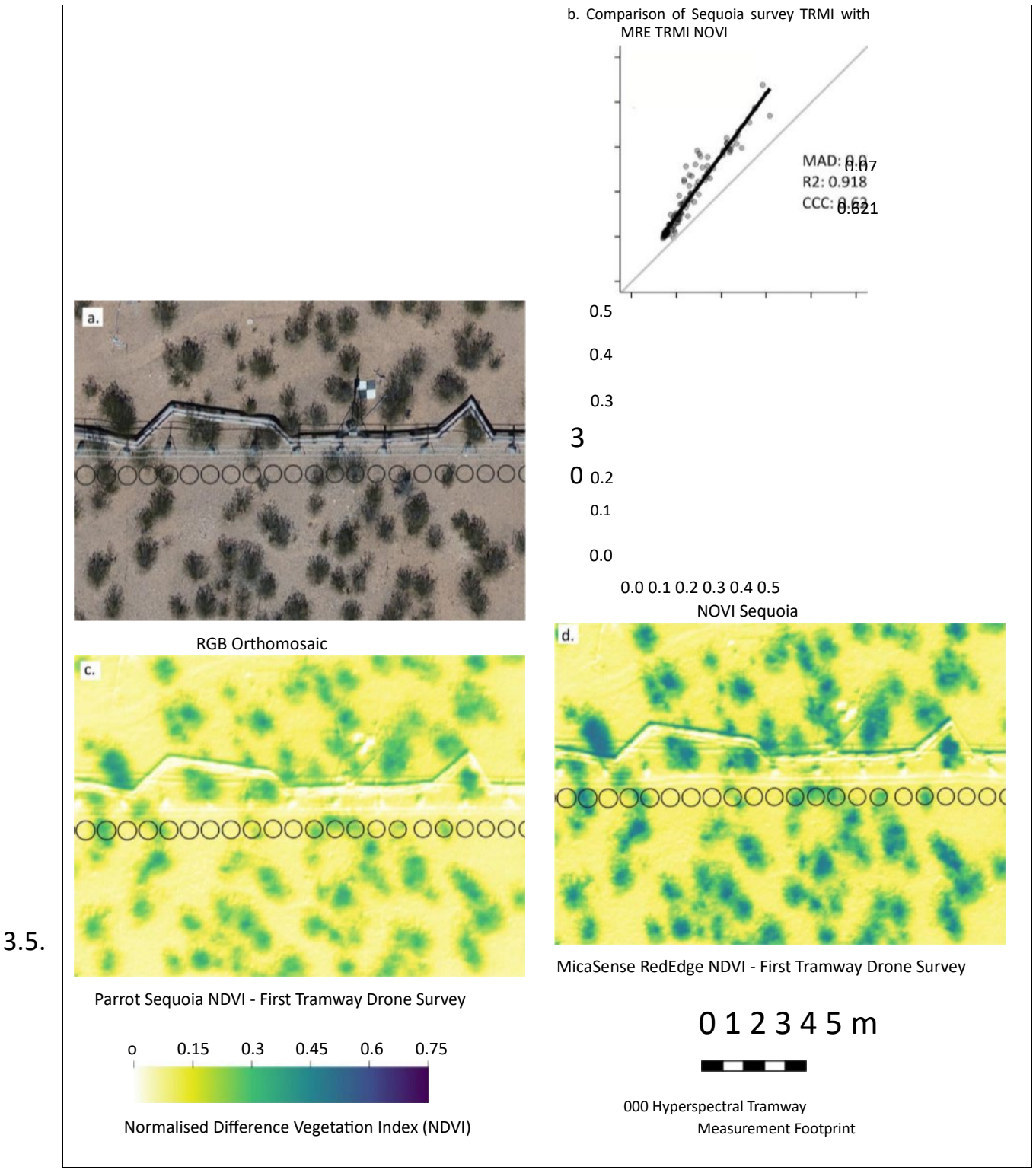


Fig. 5. Comparison of drone-derived NDVI from Parrot Sequoia and MicaSense RedEdge surveys TRM 1, demonstrating the higher NDVI values obtained from the MRE survey. RGB orthomosaic (a), comparison plot of extracted NDVI for each tramway measurement footprint derived from PS and MRE surveys (b), NDVI image data from PS survey TRMI (c), NDVI image data derived from MRE survey TRMI (d). Mean absolute deviation (MAD), coefficient of determination (R²), and Lin's concordance

Fig. correlation coefficient (CCC) values are presented.

the 2.6 ha ARE_I area are presented in Fig. 8 and Table 5. The range of a variogram is the lag at which



Spatial grain of semivariance in spectral reflectance

0

Results of the geostatistical analysis applied to NDVI data from PS and MRE drone image survey data over

semivariance reaches a plateau irrespective of further increases in separation distance, with the "sill variance" being the semi-variance value at the range (and an indicator of the total amount of spatial variation

Drone Appl. 1-27 (2023) dx.doi.org/10.1139/dsa-2023-0003

Canadian Science Publishing

present). Nugget variance is the model intercept and is related to measurement error and noise. As data become more spatially clustered, the range is expected to increase (Isaaks and Srivastava 1989). The values obtained from a fitted model show that both sensors had similar "range" values of 1.76 m (PS) and 1.82 m (MRE). This indicates that the textural grain of spatial variation in NDVI is of this order. The sill variance is much greater for the MRE sensor compared with the PS (0.0105 vs. 0.0048, respectively), showing that the total amount of spatial variation in NDVI measured by the MRE sensor was greater than in the PS data (e.g., maximum NDVI was higher in MRE than in PS).

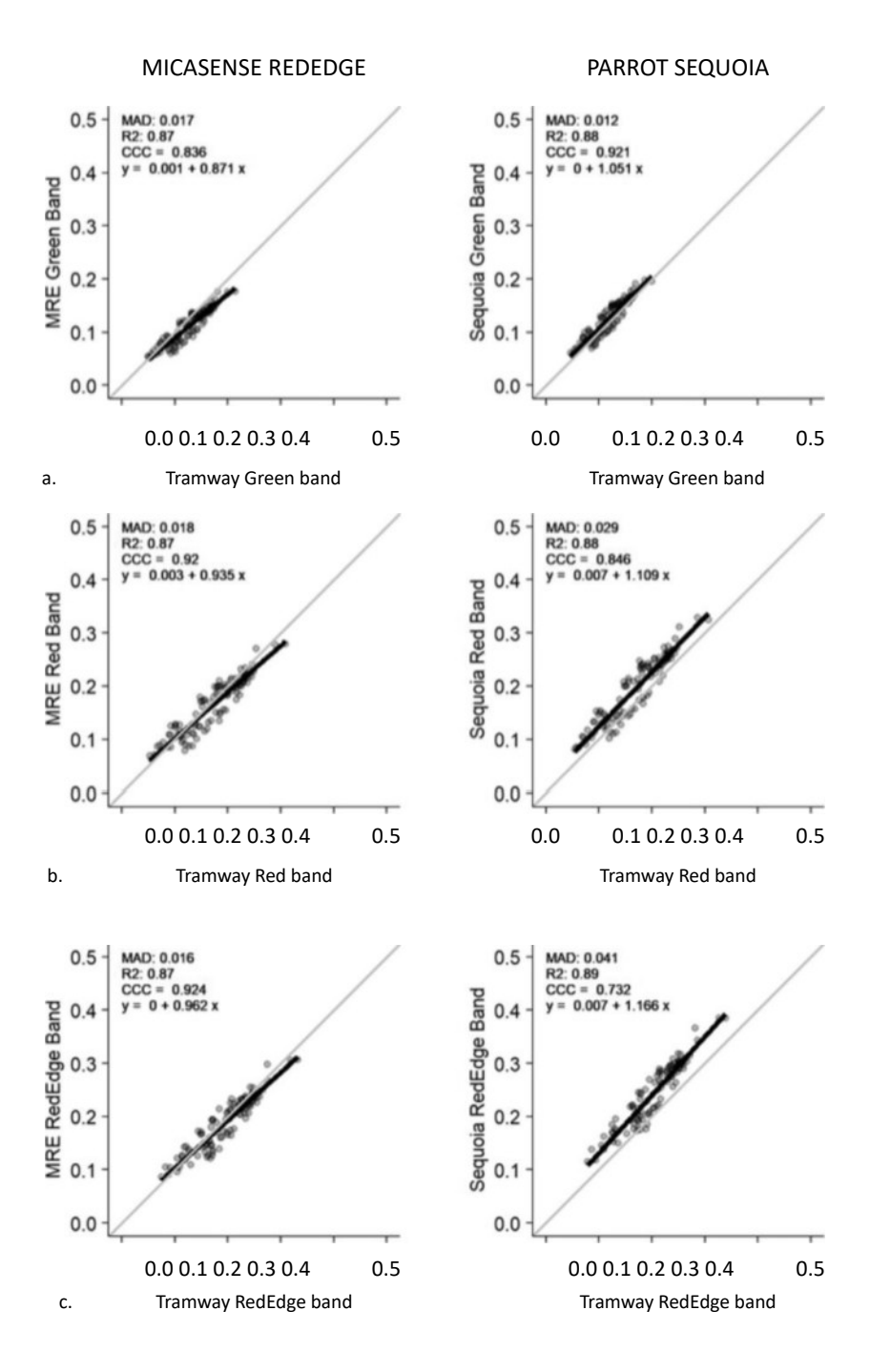
3.6. Intercomparison of sulface reflectance derived from Sentinel-2 and drone image data

Plots of comparison betw^meen drone and Sentinel-2 derived surface reflectance values are given in Fig. S17 and Fig. S19 for PS and MRE sensors, respectively, with the statistical

0

0

6. Mean surface reflectance of tramway footprints for (a) green, (b) red, (c) red edge, and (d) near-infrared (NIR) bands compared between drone-acquired MRE (MicaSense RedEdge) and PS (Parrot Sequoia) image data and tramway hyperspectral measurements. Tramway data were resampled to the wavelength band of the corresponding drone sensor. Mean absolute deviation (MAD), coefficient of determination (R²), and Lin's concordance correlation coefficient (CCC) values are presented.



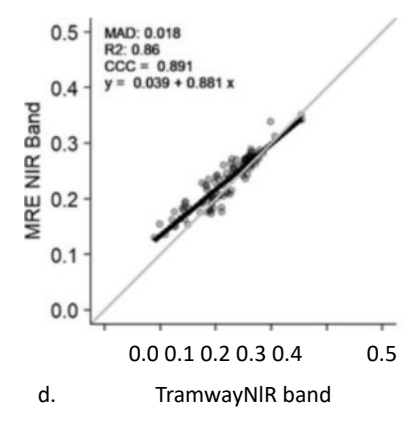


Table 3. Mean drone sensed reflectance—summary statistics for intercomparison of Sequoia and MicaSense RedEdge measurements with hyperspectral measurements from tramway.

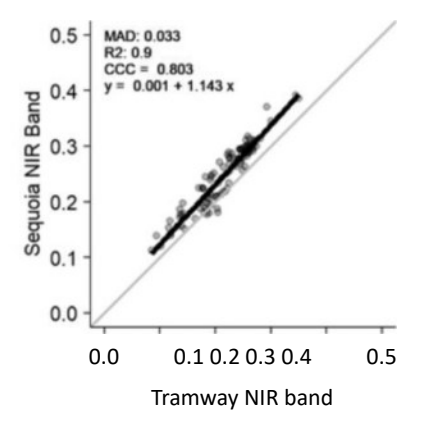
	Parrot Sequoia compared with hyperspectral measurements		MicaSens RedEdg compar hypersp measure	ge red with pectral
	CCC		CCC	
Blue			0.842	0.011
Green	0.921	0.012	0.836	0.017
Red	0.846	0.029	0.920	0.018
Red Edge	0.732	0.041	0.924	0.016
NIR	0.803	0.033	0.891	0.018
NDVI	0.868	0.024	0.677	0.061

o Note: Mean absolute deviation (MAD) and Lin's concordance correlation co• efficient (CCC) values are presented.

analysis of each band summarised in Table 6. The RedEdge wavelengths in Sentinel-2 data have a spatial resolution of 20 m sensed in three bands (Table SI—B5, B6, and B7); the PS RedEdge sensor was compared against Sentinel-2 Band 6 and the MRE against Sentinel-2 Bands 5 and 6 in Fig. S18.

The PS and Sentinel-2 reflectance measurements have a low MAD across all sensor bands (MAD: 0.009 to 0.015) (Fig. S17 and Table 6). The CCC measure of agreement between the PS and Sentinel-2 data was between 0.515 and 0.813 for the band sensor data and was 0.259 for NDVI.

The MRE sensors have a negative bias compared with Sentinel-2 data in all bands, with MAD values of between 0.020 and 0.027. The CCC values for the agreement between MRE and Sentinel-2 data were lower than for the PS comparison, ranging between 0.127 and 0.366. Due to the lower variance in the data at this spatial resolution, the values were more clustered, making it difficult to fit a robust linear model to describe the relationship between Sentinel-2 and drone-acquired data. The PS-derived NDVI plots (Fig. S18) in 0 dicate broadly similar values to Sentinel-2



NDVI values; however, the MRE-derived NDVI values (Fig. S19) are consistently higher than Sentinel-2 data. Figure 9 demonstrates how, at the 10 m spatial resolution of the Sentinel-2 image data, the variation in surface reflectance is lower than at the drone image resolution, and the resulting coarser scale NDVI image data conveys less information on the spatial heterogeneity of the vegetation.

3.7. Intercomparison of vegetation indices derived from Sentinel-2 and drone image data

Vegetation indices derived from Sentinel-2 data were compared with drone image data aggregated to the same pixel extent in the plots presented in Fig. S20. The low data variability at the spatial scale of the Sentinel-2 data meant that there is very limited inference space for intercomparison, and it is difficult to fit linear models to the plotted data in derived vegetation indices, which is reflected in the R² and CCC values (Fig. S20 and Table 7). Acknowledging these limitations, there was good correspondence between drone and Sentinel2-derived vegetation indices, as indicated by the MAD values (Table 7).

3.8. Comparison between drone-derived FVC and vegetation indices flom satellite data

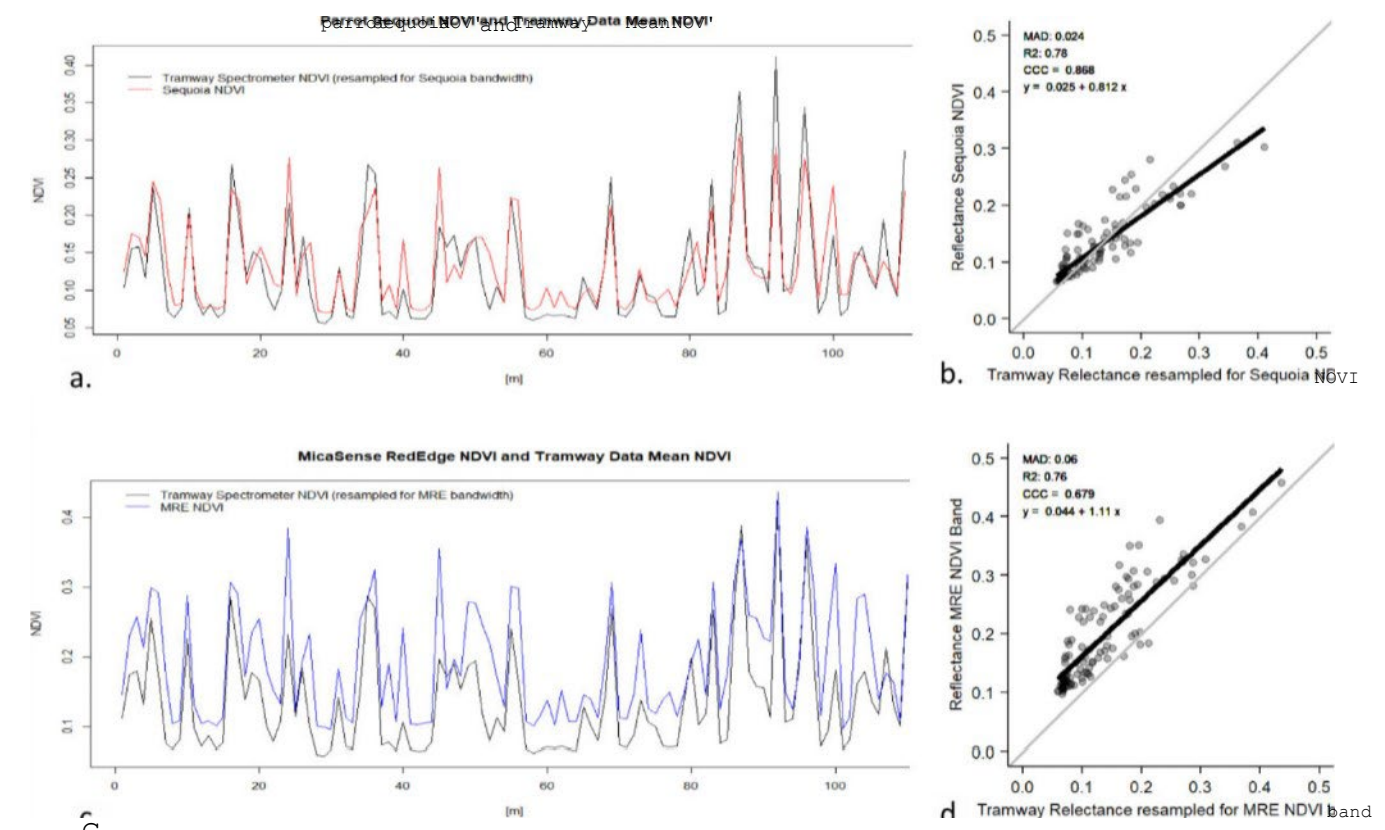
The random forest machine learning-derived classified vegetation cover map for the wider study area (ARE_I) and the resulting downscaled PVC for Sentinel-2 (10 m spatial resolution) pixel footprints are presented in Fig. S21. The overall WC for the wider study area is 29.75%, with PVC in Sentinel2 pixels ranging from 12.9% to 55%. Comparison plots of Sentinel-2 NDVI and MSAV12 with WC for each pixel presented in Fig. S22 show a poor correspondence (MAD: 0.163 and 0.211; CCC: 0.023 and 0.003, respectively) between vegetation indices and FVC at 10 m spatial resolution. To investigate whether correspondence was improved by using finer-resolution satellite data, we performed a separate comparison using PlanetScope (3 m spatial resolution) image data. The FVC

Fig.

results with NDVIIMSAV12 comparisons are presented in Fig. S23. The comparison plots of PlanetScope NDVI and MSAV12 presented in Fig. S23 also show a similar low correspondence with FVC (MAD: 0.215 and 0.161; CCC: 0.015 and 0.038, respectively)

range of interesting complexities arise from the grainvarying comparisons. Using these multiscale datasets in concert with each other allowed us to address questions regarding data correspondence across scales. Our

7. Parrot Sequoia NDVI plotted along tramway length against hyperspectral measurements resampled to the same spectral resolution. (a) Comparison plot of Parrot Sequoia-derived NDVI against hyperspectral measurements for the same footprints; (b) MicaSense RedEdge NDVI plotted along tramway length against hyperspectral measurements resampled to the same spectral resolution; and (c) comparison plot of MicaSense RedEdge derived NDVI against hyperspectral measurements for the same footprints.



at the finer grain of the 3 m pixel resolution. The low band importance scores (0.00915) for NDVI from the random forest machine learning algorithm (Fig. S21e) indicate that this VI was not an important predictor for discriminating vegetation cover in this classifier.

4. Discussion

We present the results of a unique experiment that combines transect-based hyperspectral measurements of surface reflectance factors with simultaneously captured (reflectance-calibrated) dronemounted MCA sensor data and near-time satellite observations. In doing so, we responded directly to Gamon et al. (2006b) and Gamon (2015), whose work called for such experiments to bridge the scaling gap, and Sun et al.'s (2021) work, which highlighted these endeavours as enabling basic ecological questions to be answered across multiple scales. Furthermore, we did so in a low-biomass dryland setting, which is understudied globally. We show that a discussion is structured according to the four questions posed at the start of the experiment.

4.1. Reproducibility within and correspondence between MRE and PS sensors

The reproducibility ufthin each of the MRE and PS datasets (n = 3) suggests that these sensors can reliably reproduce results in dryland conditions and therefore appear suitable for use in comparison studies of different sites and over different time scales. Achieving this reproducibility requires standard Table 4. Summary statistical table of analysis of different vegetation indices derived from droneacquired image data compared with tramwav measurements.

ſ	١	۱	
ı	ı	۱	
١,			

Canadian Science Publishing Parrot Sequoia compared with hyperspectral measurements		MicaSens RedEdg compar hypersp measur	ge red with pectral	
	CCC		CCC	
	0.868	0.024	0.679	0.061
SAVI	0.858	0.012	0.567	0.036
MSAV12	0.846	0.011	0.538	0.032
MTVI2	0.820	0.017	0.843	0.016

Note: Mean absolute deviation (MAD) and Lin's concordance correlation cc» effcient (CCC) values are presented.

protocols encompassing flight survey planning, ground control, sensor calibration, and image processing.

All the surveys were conducted in similar cloud-free weather conditions, with a small variation in solar elevations ranging from 43.2 to 48 degrees. Further investigation would be required to assess whether the same drone sensors would produce similar results when acquiring data under a wider range of solar elevation and cloud conditions or over longer time periods. Furthermore, we did not test the long-term radiometric stability of the MCA sensors, and it is reported elsewhere that the PS sensor is prone to temperaturedependent shifts in sensitivity (Olsson et al. 2021). We did follow Olsson et al.'s (2021) suggestion to allow both MCA sensors a warming-up period of 1 min prior to data acquisition, but it is plausible to suggest that sensor operations through the growing season in different air temperature conditions could impact data quality over longer timescales.

Between the MRE and PS datasets, we found important differences. The MRE sensor produced reflectance data that were generally lower in all bands than the PS sensor, with the calculated NDVI being higher when derived from the MRE sensor than the PS. This higher NDVI can be partially explained by the different wavelength positions and widths sampled by the two sensors. The comparison of NDVI generated by resampling the hyperspectral data to the different sensor response curves (Fig. S7) demonstrates that the bandwidths sampled by the MRE sensors result in higher NDVI values than for the PS band widths. However, this difference in sampled bands alone does not appear to fully explain the higher positive bias of the MRE-derived NDVI relative to the PS image data. Investigators should be mindful that the data from the two sensors are not directly equivalent, especially

Fig.

0

8. Experimental semivariogram of Parrot Sequoia and MicaSense RedEdge derived NDVI image data over the wider area (2.6 ha) survey (ARE I).

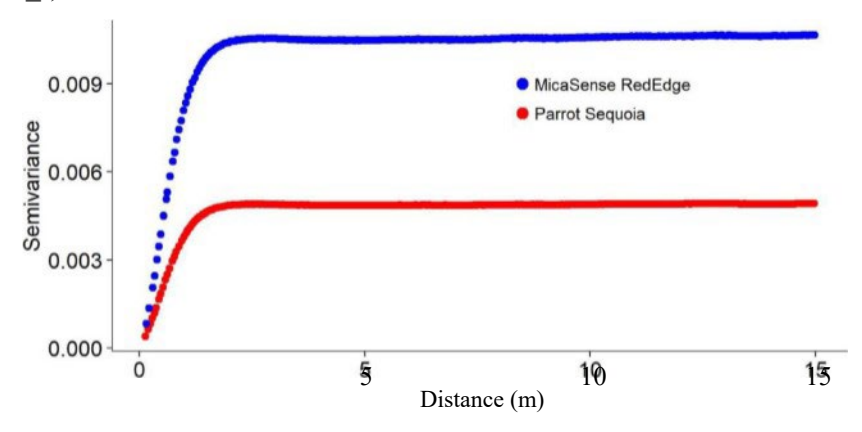


Table 5. Results of semi-variogram analysis taken from fitted model.

Variogram	Parrot Sequoia NDVI	MicaSense RedEdge NDVI
Lag (unit distance sampled)	0.0663	0.0742
	1.7698	1.8206
Sill	0.0048	0.0105
Nugget		

Table 6. Summary table—statistical comparison between Sentinel-2 image data and drone-derived image data

Sentinel-2	Parrot Sequoia compared with Sentinel-2 measurements		compar	nel-2
Band	ccc		ccc	
Blue Green Red Red Edge B5 Red Edge B6	0.541 0.789 0.515 0.813 0.259	0.011 0.009 0.015 0.009 0.013	0.154 0.294 0.366 0.246 0.127 0.420 0.217	0.020 0.021 0.027 0.028 0.043 0.024 0.025

resampled to the pixel grain of Sentinel-2 image.

Note: Mean absolute deviation (MAD) and Lin's concordance correlation co-effcient (CCC) values are presented.

in higher level products such as NDVI, which can ampli\$' differences. As a note of caution—we suggest that if others wish to combine data from twoo different mini-MCA sensors we advocate for ecosystem-specific adjustment factors (e.g., based on Fig. 4b or the resampled tramway spectra comparisons in Figs. S8—S16), but we suggest that these would need further investigation across a greater range of conditions than tested here. Such correction factors are commonly used in satellite RS studies to translate data and products between sensors with different radiometric characteristics (e.g., Roy et al. 2016; Fassnacht et al. 2019), but the process of doing so with drone datasets has been less well explored and likely has different constraints (fewer corresponding observations, for example).

4.2. Relationship between drone-acquired multispectral reflectance products and field reflectance factor measurements from the tramway-mounted spectroradiometer

Drone-derived reflectance products and tramway-derived hyperspectral reflectance data produced different results, with the difference more pronounced in higher level products such as NDVI. The PS-derived reflectance values were higher than the field-based hyperspectral measurement (by betw•een 5% and 16%), a result consistent with other vegetation studies using the PS sensor (Fawcett et al. 2020). MRE sensor-recorded radiance was lower compared with field spectroradiometer measurements (by betw•een 4% and 13%) consistent with other studies using an MRE sensor (Padrö et al. 2018). The calculated NDVI for the PS system had a pattern and magnitude of deviation similar to those found by Fawcett et al. (2020). The consistent positive bias in NDVI derived from the MRE sensor was of a larger deviation than the hyperspectral tramway measurements (ca. 11 %). We posit that

these differences were caused by a combination of the following factors:

- (a) Uncertainties in the projected footprints of the tramway spectroradiometer at each measurement location, which should be a random effect and relatively low order.
- (b) Spatial mismatch between the predicted conical footprint view of the spectroradiometer and the circular extract captured from the drone orthomosaics. We expect that in the heterogenous dryland system, this might lead
- 9. Example of Mica Sense Red Edge (MRE) (a) and Parrot Sequoia (PS) NDVI (c) image data resampled to the spatial resolution of Sentinel-2 (10 m) (b and d, respectively). Corresponding NDVI image from Sentinel-2 image data (e).

Fig.

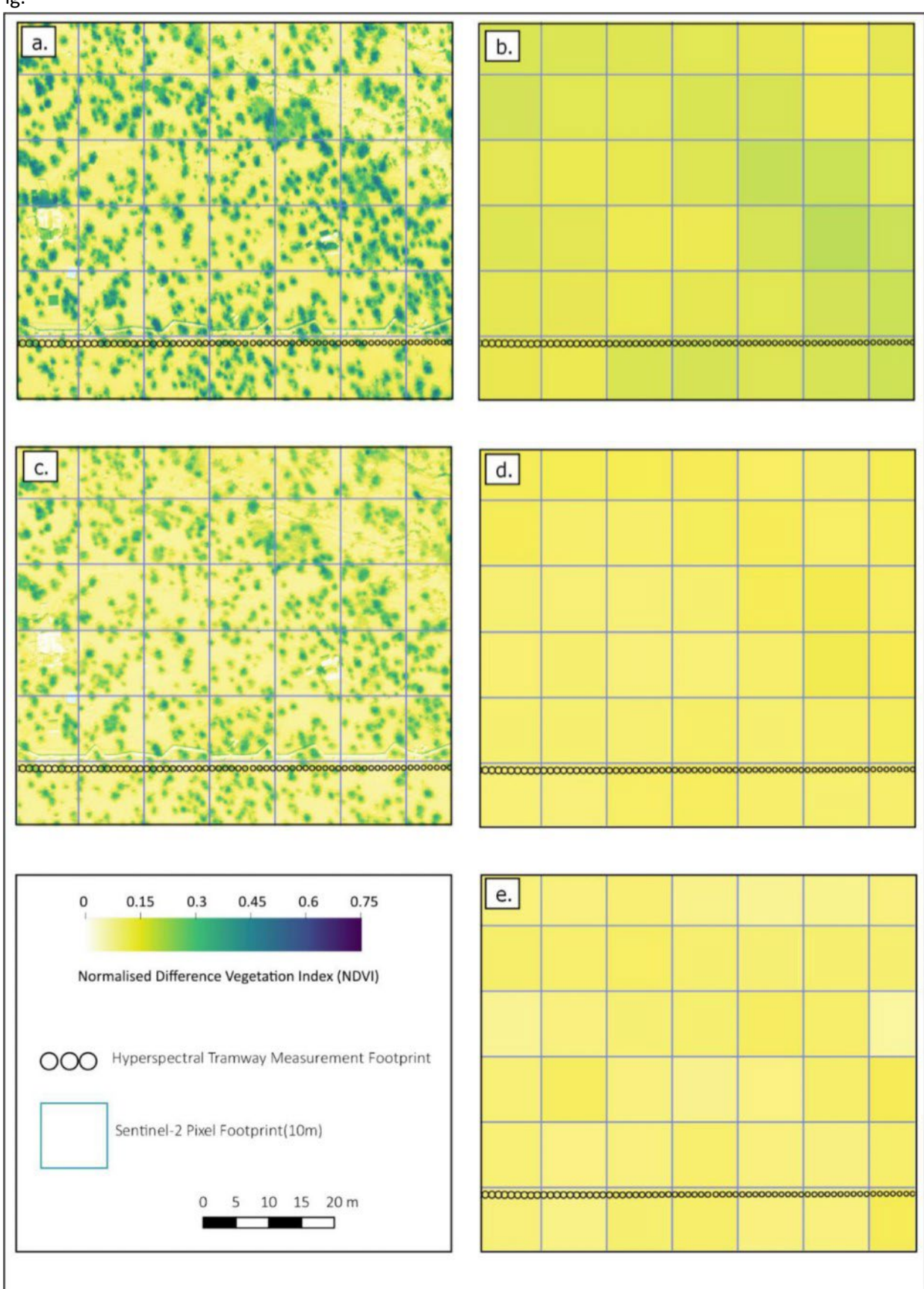


Table 7. Summary table—statistical comparison between Sentinel-2 image data and drone-derived vegetation indices.

Sentinel-2	Parrot compar Senti measure	nel-2	MicaSens RedEdg compare Senti measure	ge ed with nel-2
	CCC	MAD	CCC	
NDVI	0.259	0.013	0.217	0.025
SAVI	0.117	0.008	0.119	0.014
MSAV12	0.098	0.007	0.12	0.01
	0.103	0.017	0.214	0.013

Note: Mean absolute deviation (MAD) and Lin's concordance correlation coefficient (CCC) values are presented.

- o to different proportions of bare ground vs. vegetation within the drone-modelled field-of-view compared with the spectroradiometer data, and therefore might introduce a systematic bias caused by soil contamination of vegetation spectral signatures. Given that we found soiladjusted VIS (SAVI and MSAV12; Table 2) to show less variation compared with NDVI, this seems a plausible explanation.
 - (c) Adjacency and atmospheric effects in drone and satellite data might be expected to exert some impacts, particularly in relation to the comparison of proximal sensing to RS data from Sentinel-2. We argue that at drone level and below, atmospheric uncertainties should be negligible because of the regularity with which measurements were calibrated, and because of the clarity of the atmospheric conditions on the day of the experiment.
 - (d) For the MCA sensors, we used manufacturer-supplied spectral response functions, which may not have perfectly represented the full width and half maximum (FWHM) and central wavelengths of each band, since every sensor is slightly variable compared with generalised specifications. We expect this to have had a small impact 0 but may partially explain the biases between MCA sensors. Similarly, sensor-specific calibration uncertainties, which are difficult to untangle, may have added to this uncertainty. These two factors could explain some of the differences between the two drone-mounted sensors.

Following Cunliffe et al. (2020), we assert that it is crucial for researchers developing transfer functions betw^meen NDVI and other ecological or biophysical attributes (e.g., AGB or gas fluxes) to evaluate the potential impact of these variations and uncertainties on results. Using alternative vegetation indices could be expected to affect the correspondence between spectroscopic and drone-acquired reflectance products. Crucially, in this experiment, we assert

that the spatial sampling pattern of the transect imposed a regularity on the measurements, which limited the questions that could be answered. Future experiments engaging with tramway-mounted spectrometers such as this could explore more diverse ways of capturing spectral data (focusing on spectral endmembers describing particular species or land cover types, for example), which would enable questions on reflectance and biophysical processes to be investigated at a plant species level.

4.3. What is the spatial grain of semivariance in spectral reflectance?

Scaling up from ground-based observations to drones and then to satellite data requires an understanding of the effects of the spatial scale of observation as well as the relative performance of spectral sensors. The importance of observation scales for gathering useful information on ecological spatial processes and spatial differences is well known (Dungan et al. 2002; Wagner and Fortin 2005; Jackson and Fahrig 2015). The spatial scaling issue is identified as one of the most important in remote sensing (Wu and Li 2009) and a major cause of uncertainty within the results of remote sensing studies (Lechner et al. 2012). Our results corroborate this and evidence the complexity of comparing optical signals across different spatial grains.

The heterogeneity of the dryland vegetation at different spatial grains is demonstrated by our variogram analysis of the drone-derived image data. At spatial resolutions greater than ca. 1.8 m, the variability in the system is mostly lost, and this ecosystem appears more homogeneous. Our analysis of FVC at Sentinel-2 (10 m) and PlanetScope (3 m) spatial resolutions also indicates a poor ability to relate vegetation indices to plant fractional cover in these dry season conditions at coarser grains. Recently, Taylor et al. (2021) demonstrated that to be able to consistently detect land surface phen010U in a dryland ecosystem, fractional cover of up to 60% was required within a pixel. Following the framework proposed by Strahler et al. (1986), our multiscale study covers the transition between fine grain, where individual features are larger in extent than the sensing spatial resolution (i.e., tramway and drone data), and coarse grain, where features are smaller than the sensing resolution (i.e., satellite data). Strahler et al. (1986) suggested that spatial domains that occur across this finecoarse transition may require the formulation of models specific to the actual sizes of elements and resolution cells. We contend that modelling the spatial and spectral upscaling between drone and satellite data remains an important research priority for these heterogeneous dryland ecosystems.

Fig.

4.4. Correspondence of vegetation indices between drone-captured and Sentinel-2 data

In broad terms, drone-captured image data produces similar reflectance data for wavelength bands and vegetation index values to Sentinel-2 image data. The PS sensor had the greatest agreement with Sentinel-2 image data. The MRE sensor had a negative bias compared with the Sentinel-2 image data, following a similar trend to that exhibited when comparing with field-based measurements. As discussed in Section 4.3, at Sentinel-2 resolution (10 m pixel size), the ability to detect and measure spatial variability in this dryland ecosystem under winter conditions is greatly reduced, and consequently, the results for different vegetation indices do not allow us to derive inferences about their relative

usefulness for characterising this dryland ecosystem in the dry season.

4.5. Avenues for further investigation

A key reflection on this experiment relates to the spatial sampling of spectral data by the tramway. This tramway was constructed to replicate the experiment explained in Gamon et al. (2006a), where the major question was to "systematically" sample ecosystem optical properties. In addressing that question, the tramway is configured to capture spectral measurements at regular intervals of 1 m to deliver an unbiased sample of the dryland structure. This precludes the capability to measure examples of "pure" spectral endmembers, since most of the tramway sampling locations gave footprints that included mixtures of bare soil and vegetation elements. Indeed, bare ground was the dominant (> 50%) cover type in 63% o

u of the tramway hyperspectral measurements (note: broadly similar to the 29.75% PVC calculated for the study area; Fig. S22b). Therefore, it was not possible to perform an analysis of the reflectance data at the plant species level since there were insufficient pure plant samples for endmember analysis. Further work with the tramway to address different questions about seasonal and spatial variations in pure plant specieslsoil spectral endmembers could be undertaken with different stopping points along the transect programmed to coincide with ideally 100% singlespecies plant cover or 100% bare soil. Furthermore, given that the tramway instrument executes a two-way journey (out and back) to deliver replication, in the future the instrument could be configured to sample plantlsoil endmembers on the return journey to address different questions.

A further avenue for investigation would be to repeat the intercomparison of hyperspectral, drone, and satellite measurements during different landscape phenophases. An intercomparison of peak biomass conditions during the wet season would be valuable to assess whether the results from this study are reproduced at higher greenness levels. Additional studies at different times of the year would also address questions relating to the ability of drone and satellite sensors to 0 detect vegetation anomalies and capture temporal changes in these dryland ecosystems.

In addition to nadir measurements such as those from the tramway, future work might also consider the suggestions of Wardley et al. (1987), who queried the spatial and spectral complexities of scene models over heterogeneous vegetation. They explain that information such as the threedimensional form of the spectral reflectance function (e.g., approximation of the bidirectional reflectance distribution function (i.e., more than nadir measurements)), and spatial information on the geometric arrangement of canopy components is required to build improved scene models. Furthermore, they suggest that temporal dynamics need to be captured, and spectral tramways such as the one used here offer an ideal vehicle from which to fill this knowledge gap.

5. Conclusion

Using radiometrically calibrated data from two multispectral drone sensors (MRE and PS) colocated with a transect

syst.Appl.: dx.doi.orq/10.1 139/dsa-2023-0003

of hyperspectral measurements (tramway), we found that drone-based multispectral sensors capture data at the necessary fine spatial and spectral resolution to provide useful information characterising this dryland ecosystem in the dry season. We found that data collected by the same drone sensors had a strong spectral similarity, but that reflectance measurements and vegetation indices (NDVI, MTV12, MSAVI2, and SAVI) varied between field, drone, and satellite sensors. We conclude that investigators using data from different sensors need to account for biases in the spectral sensitivity of the sensors. Analysis of satellite image data at 3 m (PlanetScope) and 10 m (Sentinel-2) resolution showed that the spectral range in the data was reduced compared with drone data, and the variogram analysis of NDVI derived from the drone data found that ecological pattern information was lost at grains coarser than 1.8 m. These findings suggest that in the dry season in this dryland ecosystem, sensor spatial resolutions should be finer than 1.8 m to capture relevant ecological information.

The intercomparison of hyperspectral, drone, and satellite data presented in this paper helps to interpret satellite data, such as those from PlanetScope and Sentinel-2, that have too coarse spatial resolutions for capturing important ecological patterns. We conclude that modelling spatial and spectral upscaling between drone and satellite data remains a complex yet important research priority for these heterogeneous chyland ecosystems.

Acknowledgements

We thank Dr. Fabio Boschetti for assistance with data collection, and John Anderson for assistance with logistics. We acknowledge the support of PI Craig Tweedie from UTEP who established the tramway infrastructure in the Jornada experimental range. We thank Dr. Carl Salvaggio and Dr. Baabak Mamaghani for sharing sensor response function data for the MicaSense RedEdge-M instrument. We are grateful to Prof. Stephen Sitch and Dr. Tim Hill for their collaboration on the wider NERC-funded Driving-C project that provided the core funding for this work.

Article information

Histoly dates

Received: 27 January 2023 Accepted: 5 June 2023

Accepted manuscript online: 6 June 2023 Version of record online: 3 July 2023

Copyright

0 2023 The Author(s). This work is licensed under a Creative Commons Attribution 4.0 International License (CC BY 4.0), which permits unrestricted use, distribution, and reproduction in any medium, provided the original author(s) and source are credited.

Data availability https://lzenodo.org/badgellatestdoi1501316875

17

Author information

Author ORCIDs

Glenn Slade https:llorcid.org/0000-0003-3305-9554
Dominic Fawcett https:llorcid.org/0000-0002-0159-2533
Andrew M. Cunliffe https:llorcid.org/0000-0002-8346-4278
Richard E. Brazier https:llorcid.org/0000-0002-8715-0399
Kamal Nyaupane https:llorcid.org/0000-0002-8273-6833
Marguerite Mauritz https://orcid.org/0000-0001-8733-9119
Sergio Vargas https://orcid.org/0000-0002-0052-8580
KarenAnderson https://orcid.org/0000-0002-3289-2598

Author notes

Karen Anderson served as an Editor-in-Chief at the time of manuscript review and acceptance; peer review and editorial o u decisions regarding this manuscript were handled by another

Editorial Board Member.

Author contributions

Conceptualisation: DF, AMC, Data curation: DF, AMC, KN.

KA o KA

> Formal analysis: GS, DF, AMC, KA Funding acquisition: AMC, REB. KA Investigation: GS. DF. AMC, MM, KA

Methodology: GS, DF, AMC, KA

Project administration: AMC, REB, KA

Resources: KA

Supervision: AMC, KA

Visualisation: GS, DE, AMC, KA

Writing - original draft: GS, DF, AMC, KA

Writing - review & editing: GS, DF, AMC, REB, KN, MM,

SV,

Competing interests

The authors declare that there are no competing interests.

_

Funding information

RB, AC, KA, DF, and GS were supported by the Natural En . vironment Research Council (NERC) (NEIR00062X11). AC was supported by the Oppenheimer Programme in African Landscape Systems (OPALS) funded by the Oppenheimer Generations Research and Conservation (OGRC), University of Exeter and Sarah Turvill. DF received funding from the European Union's Horizon 2020 research and innovation programme under the Marie Sklodowska-Curie Grant Agreement No. 721995. The UTEP team (MM, SV, and and the site at which the tramway is located were supported under NSF Grants: 1242122, 0734825, 0618210, 1235828, and 2025166. Current funding for MM, SV, and KT comes from the CZ Dryland grant number 2012475.

Supplementary material

Supplementary data are available with the article at https: 11doi.org110.11391dsa-2023-0003.

References

Ahlström, A, Raupach, M.R., Schurgers, G., Smith, B., Arneth, A, Jung, M., et al. 2015. The dominant role ofsemi-arid ecosystems in the trend and variability of the land C02 sink. Science, 348: 895—899. doi:10.11261science.aaa1668. PMID: 25999504.

Assmann, J.J., Kerby, J.T., Cunliffe, A.M., and Myers-Smith, I.H. 2018. Vegetation monitoring using multispectral sensors—best practices and lessons learned from high latitudes. J. Unmanned Veh. Syst. doi:10.11391juvs-2018-0018.

Assmann, JJ., Myers-Smith, I.H., Kerby, J.T., Cunliffe, A.M., and Daskalova, G.N. 2020. Drone data reveal heterogeneity in Tundra greenness and phenology not captured by satellites. Environ. Res. lett. 15: 125002. doi:10.1088/1748-9326/abbf7d.

Baston, D. , ISciences, LLC 2022. exactextractr: fast extraction from Raster Datasets using polygons.

Biederman, JA, Scott, R.L., Bell, T.W., Bowling, D.R., Dore, S., GaratuzaPayan, J., et al. 2017. C02 exchange and evapotranspiration across dryland ecosystems of southwestern North America. Glob. Change

Biol. 23: 4204-4221. doi:10.1111/gcb.13686. PMID: 28295911.

Cunliffe, A.M., Brazier, R.E., and Anderson, K. 2016. Ultra-fine grain landscape-scale quantification of dryland vegetation structure with drone-acquired structure-from-motion photogrammetry. Remote Sens. Environ. 183: 129-143. doi:10.10161j.rse.2016.05.019.

Cunliffe, A.M., Assmann, J., Daskalova, G., Kerby, J.T., and Myers-Smith, I.H. 2020. Aboveground biomass corresponds strongly with dronederived canopy height but weakly with greenness (NDVI) in a shrub tundra landscape. Environ. Res. Lett. doi:10.108811748-93261aba470.

Cunliffe, A.M., Anderson, K., Boschetti, F., Brazier, R.E., Graham, HA, Myers-Smith, I.H., et al. 2022a. Global application of an unoccupied aerial vehicle photogrammeuy protocol for predicting aboveground biomass in non-forest ecosystems. Remote Sens. Ecol. Conserv. 8: 57—71. doi:10.10021rse2.228. PMID: 35873085.

Cunliffe, A.M., Boschetti, F., Clement, R., Sitch, S., Anderson, K., Duman, T., et al. 2022b. Strong correspondence in evapotranspiration and carbon dioxide fluxes between different eddy covariance systems enables quantification of landscape heterogeneity in dlyland fluxes. J. Geophys. Res.: Biogeosci. 127: e2021JG006240. doi:10.10291 2021JG006240.

D'Odorico, P., Gonsamo, A., Damm, A., and Schaepman, M.E. 2013. Experimental evaluation of Sentinel-2 spectral response filnctions for NDVI time-series continuity. IEEE Trans. Geosci. Remote Sens. 51: 1336—1348. doi:10.1109/TGRS.2012.2235447.

- Dungan, J.L., Perry, J.N., Dale, M.R.T., Legendre, P., Citron-Pousty, S., Fortin, M.-J., et al. 2002. A balanced view of scale in spatial statistical analysis. Ecography, 25: 626—640. doi:10.10341j.1600-0587.2002. 250510.x.
- ESA 2019. Sentinel-2 spectral response functions (S2-SRF) _Sentinel online version 3.0 [VS"WW Document]. Available from https:llsentinels.copernicus.eu/weblsentinel/user-guidesls entinel-2-msildocument-library/-lasset_publisher/"VVkOTKajilSaRlco ntentlsentinel-2a-spectral-responses.
- Fassnacht, F.E., Schiller, C., Kattenborn, T., Zhao, X., and Qu, J. 2019. A landsat-based vegetation trend product of the Tibetan Plateau for the time-period 1990—2018. Sci. Data, 6: 78. doi:10.1038/s41597-019-.0075-9. PMID: 31148554.
- Fawcett, D., Panigada, C., Tagliabue, G., Boschetti, M., Celesti, M., Evdokimov, A., et al. 2020. Multi-scale evaluation of drone-based multispectral surface reflectance and vegetation indices in operational conditions. Remote Sens. 12: 514. doi:10.33901rs12030514.
- Fawcett, D., Cunliffe, A.M., Sitch, S., O'Sullivan, M., Anderson, K., Brazier, R.E., et al. 2022. Assessing model predictions of carbon dynamics in global drylands. Front. Environ. Sci. 10. doi:10.33891fenvs.2022. 790200.
- Fernändez-Guisuraga, J.M., Sanz-Ablanedo, E., Suärez-Seoane, S., and Calvo, L 2018. Using unmanned aerial vehicles in postfire vegetation survey campaigns through large and heterogeneous areas: opportunities and challenges. Sensors, 18: 586. doi:10.33901s18020586. PMID: 29443914.
- Franzini, M., Ronchetti, G., Sona, G., and Casella, V. 2019. Geometric and radiometric consistency of Parrot Sequoia multispectral imagery for precision agriculture applications. Appl. Sci. 9: 5314. doi:10.3390/app9245314.
 - Gamon, JA, Cheng, Y, Claudio, H., MacKinney, L, and Sims, DA. 2006a. A mobile tram system for systematic sampling of ecosystem optical properties. Remote Sens. Environ. Spectr. Netw. 103: 246—254. doi:10.10161j.rse.2006.04.006.
 - Gamon, JA., Rahman, A.F., Dungan, J.L., Schildhauer, M., and Huemmrich, K.F. 2006b. Spectral network SpecNet)—what is it and why do we need it? Remote Sens. Environ. Spectr. Netw. 103: 227—235. doi.•10.10161j.rse.2006.04.003.
 - Gamon, JA. 2015. Reviews and syntheses: optical sampling of the flux tower footprint. Biogeosciences, 12: 4509—4523. doi:10.5194/ bg-12-4509-2015.
 - Gräler, B., Pebesma, E., and Heuvelink, G. 2016. Spatio-temporal interplation using gstat. R J. 8: 204-218. doi:10.32614/RJ-2016-014.
 - Grünzweig, J.M., De Boeck, H.J., Rey, A., Santos, M.J., Adam, 0., Bahn, M., et al. 2022. Dryland mechanisms could widely control ecosystem functioning in a drier and warmer world. Nat. Ecol. Evol. 6: 1064—1076. doi:10.10381s41559-022-01779-y. PMID: 35879539.
- Havstad, K, Huenneke, L., and Schlesinger, W.H. 2020. Structure and function of a Chihuahuan Desert ecosystem: the Jornada Basin Longo Term Ecological Research Site, Jornada Basin LTER.
- u Houghton, R., Hackler, J., and Lawrence, K. 2001. Changes in terrestrial carbon storage in the United States. 2: the role of fire and fire management. Glob. Ecol. Biogeogr. 9: 145—170. doi:10.10461j.1365-2699. 2000.00164x.
 - Isaaks, E.H., and Srivastava, R.M. 1989. Applied geostatistics. Oxford University Press.
 - Jackson, H.B., and Fahrig, L 2015. Are ecologists conducting research at the optimal scale? Glob. Ecol. Biogeogr. 24: 52—63. loi:10.111llgeb. 12233
 - Laliberte, A.S., Goforth, MA, Steele, C.M., and Rango, A. 2011. Multispectral remote sensing from unmanned aircraft: image processing workflows and applications for Rangeland environments. Remote Sens. 3: 2529-2551. doi:10.33901rs3112529.
 - Laney, C. 2013. Toward new data and information management solutions for data-intensive ecological research. doi:10.1314012.1.4595.4244.
 - Lechner, A.M., Langford, WT., Bekessy, S.A., and Jones, S.D. 2012. Are landscape ecologists addressing uncertainty in their remote sensing data? Landscape Ecol. 27:1249-1261. doi:10.10071s10980-012-9791-7.
 - Lin, L 1989. A concordance correlation coefficient to evaluate reproducibility. Biometrics, 45: 255—268. doi:10.230712532051. PMID: 2720055.
 - Lin, L. 2000. Corrections. Biometrics, 56: 324-325. doi:10.1111/j.

- 0006-341x.2000.00324x.
- Lu, H., Fan, T., Ghimire, P., and Deng, L 2020. Experimental evaluation and consistency comparison of UAV multispectral minisensors. Remote Sens. 12: 2542. doi:10.33901rs12162542.
- Mamaghani, B., and Salvaggio, C. 2019. Multispectral sensor calibration and characterization for sUAS remote sensing. Sensors, 19: 4453. 0 doi:10.33901s19204453. PMID: 31615104.
 - Mayor, Å.G., Kéfi, S., Bautista, S., Rodriguez, F., Carteni, F., and Rietkerk, M. 2013. Feedbacks between vegetation pattern and resource loss dramatically decrease ecosystem resilience and restoration potential in a simple dryland model. Landsc. Ecol. 28: 931—942. doi:10.1007/

s10980-013-9870-4.

- McBride, G. 2005. A proposal for strength-of-agreement criteria for Lin's concordance.
- McDowell, N, Pockman, WT., Allen, C.D., Breshears, DD., Cobb, N., Kolb, T., et al. 2008. Mechanisms of plant survival and mortality during drought: why do some plants survive while others succumb
 - to drought? New Phytol. 178: 719–739. doi:10.1111/j.1469-8137.2008. 02436.x. PMID: 18422905.
- McIntire, C.D., Cunliffe, A.M., Boschetti, F., and Litvak, M.E. 2022. Allometric relationships for predicting aboveground biomass, sapwood, and leaf area of two-needle pifion pine (Pinus edulis) amid opengrown conditions in Central New Mexico. For. Sci. frac001. doi:10. 10931forscilfrac001.
- Monger, C.H., Mack, G.H., Nolen, B., and Gile, L.H. 2006. Regional setting ofthe jornada basin. In Structure and function of a Chihuahuan Desert ecosystem. The Jornada Basin Long-Term Ecological Research Site. Edited By K. Havstad, L. Huenneke and W.H. Schlesinger. Oxford University Press, New York, NY. pp. 15—43.
- Nagler, P.L, Glenn, E.P., Kim, H., Emmerich, W., Scott, R.L, Huxman, T.E., and Huete, AR. 2007. Relationship between evapotranspiration and

syst App'. <u>dx.doi.org/10.1139/dsa-2023-0003</u>

- precipitation pulses in a semiarid rangeland estimated by moisture flux towers and MODIS vegetation indices. J. Arid Environ. 70: 443—462. doi:10.10161j.jaridenv.2006.12.026.
- Okin, G.S., Heras, M.M. las, Saco, P.M., Throop, H.L, Vivoni, E.R., Parsons, A.J., et al. 2015. Connectivity in dryland landscapes: shifting concepts of spatial interactions. Front. Ecol. Environ. 13: 20—27. doi:10.18901
- Olsson, P.-O., Vivekar, A., Adler, K., Garcia Millan, V.P., Koc, A., Alamrani,
 - M., and Eklundh, L 2021. Radiometric correction of multispectral UAS images: evaluating the accuracy of the Parrot Sequoia camera and sunshine sensor. Remote Sens. 13: 577. doi:10.33901rs13040577.
- Padré, J.-C., Mufioz, F.-J., Åvila, L.Å., Pesquer, L, and Pons, X. 2018. Radiometric correction of landsat-8 and Sentinel-2A scenes using drone imagery in synerw with field spectroradiometry. Remote Sens. 10: 1687. doi:10.3390/rs10111687.
- Pebesma, E.J. 2004. Multivariable geostatistics in S: the gstat package. Comput. Geosci. 30: 683-691. doi:10.10161j.cageo.2004.03.012.
- Pedregosa, F., Varoquaux, G., Gramfort, A., Michel, V., Thirion, B., Grisel,
 - 0., et al. 2011. Scikit-learn: machine learning in Python. J. Mach. Learn. Res. 12: 2825-2830.
- Poulter, B., Frank, D., Ciais, P., Myneni, R.B., Andela, N., Bi, J., etal. 2014. Contribution of semi-arid ecosystems to interannual variability of the global carbon cycle. Nature, 509: 600—603. doi:10.10381nature13376. PMID: 24847888.
- QGIS Development Team 2009. QGIS geographic information system (manual).

- R Core Team. 2021. R: a language and environment for statistical computing. R Foundation for Statistical Computing, Vienna, Austria.
- Rango, A., Ritchie, J., Schmugge, T.J., Kustas, W.P., and Chopping, M. 2006. Applications of remotely sensed data from the Jornada basin. In Structure and function of a Chihuahuan Desert ecosystem: the Jornada Basin Long-Term Ecological Research Site. Edited by K. Havstad, L Huenneke and W.H. Schlesinger. Oxford University Press, New York, NY. pp. 305-320.
- Roy, D.P., Kovalskyy, V., Zhang, H.K., Vermote, E.F., Yan, L, Kumar, S.S., and Egorov, A. 2016. Characterization of Landsat-7 to Landsat-8 reflective wavelength and normalized difference vegetation index continuity. Remote sensing of environment, Landsat 8 Sci. Results, 185: 57-70. doi:10.10161j.rse.2015.12.024.
- Rufin, P., Frantz, D., Yan, L, and Hostert, P. 2021. Operational coregistration of the Sentinel-2A/B image archive using multitemporal landsat spectral averages. IEEE Geosci. Remote Sens. Lett 18: 712—716. doi:10.11091LGRS.2020.2982245.
- Safriel, U., and Adeel, Z. 2005. Dryland systems. In Millenium ecosystem assessment, ecosystems and human well-being: current state and trends. Volume 1. Edited by R. Hassan, R. Scholes and N. Ash. p. 623—662.
- Sankey, T.Ts., Leonard, J.M., and Moore, M.M. 2019. Unmanned aerial vehicle—based rangeland monitoring: examining a century of vegetation changes. Rangeland Ecol. Manage. 72: 858—863. doi:10.10161 j.rama.2019.04.002.
- Schaepman-Strub, G., Schaepman, M.E., Painter, T.H., Dangel, S., and Martonchik, J.V. 2006. Reflectance quantities in optical remote sensing—definitions and case studies. Remote Sens. Environ. 103: 27-42. doi:10.10161j.rse.2006.03.002.
- Schlesinger, W.H., and Pilmanis, A.M. 1998. Plant—soil interactions in deserts. Biogeochemistry, 42: 169—187. doi:10.10231A: 1005939924434.
- Schlesinger, W.H., Belnap, J., and Marion, G. 2009. On carbon sequestration in desert ecosystems. Glob. Change Biol. 15: 1488—1490. doi:10.

1111/j.1365-2486.2008.01763.x.

- Signorell Andri et Multi. 2022. DescTools: tools for descriptive statistics. Sitch, S., Friedlingstein, P., Gruber, N., Jones, S.D., Murray-Tortarolo, G., Ahlström, A, et al. 2015. Recent trends and drivers of regional sources and sinks of carbon dioxide. Biogeosciences, 12: 653—679. doi:10.51941bg-12-653-2015.
- Smith, W.K., Dannenberg, M.P., Yan, D., Herrmann, S., Barnes, M.L., Barron-Gafford, GA., et al. 2019. Remote sensing of dryland ecosystem structure and function: progress, challenges, and opportunities. Remote Sens. Environ. 233: 111401. doi:10.10161j.rse.2019.111401.
- Strahler, A.H., Woodcock, C.E., and Smith, JA. 1986. On the nature of models in remote sensing. Remote Sens. Environ. 20: 121—139. doi:1 O.

1016/0034-4257(86)90018-0.

19

0

- Sun, Z., Wang, X., Wang, Z., Yang, L, Xie, Y., and Huang, Y. 2021. UAVs as remote sensing platforms in plant ecology. review of applications and challenges. J. Plant Ecol. 14: 1003—1023. doi:10.10931jpe/rtab089.
- Swetnam, T.L, Gillan, J.K., Sankey, T.T., McClaran, M.P., Nichols, M.H., Heilman, P., and McVay, J. 2018. Considerations for achieving crossplatform point cloud data fusion across different dryland ecosystem structural states. Front. Plant Sci. 8. doi:10.33891fpls.2017.02144. PMID: 29379511.
- Taylor, S.D., Browning, D.M., Baca, R.A., and Gao, F. 2021. Constraints and opportunities for detecting land surface phenolow in drylands. J. Remote sens. 2021. doi:10.34133/2021/9859103.
- Thomey, M.L., Collins, S.L, Vargas, R., Johnson, J.E., Brown, R.F., Natvig, D.O., and Friggens, M.T. 2011. Effect of precipitation variability on net primary production and soil respiration in a Chihuahuan Desert

- grassland. Glob. Change Biol. 17: 1505–1515. doi:10.1111/j.1365-2486. 2010.02363.x.
- Vargas, R., Collins, S.L, Thomey, M.L, Johnson, J.E., Browen, R.F., Natvig, DO., and Friggens, MT. 2012. Precipitation variability and fire influence the temporal dynamics of soil C02 efflux in an arid grass
 - land. Glob. Change Biol. 18: 1401-1411. doi:10.1111/j.1365-2486. 2011.02628.x.
- Wagner, H.H., and Fortin, M.-J. 2005. Spatial analysis of landscapes: concepts and statistics. Ecology, 86: 1975—1987. doi:10.1890104-0914.
- Wardley, N.W., Milton, E.J., and Hill, C.T. 1987. Remote sensing of structurally complex semi-natural vegetation—an example from heathland. Int. J. Remote sens. 8: 31-42. doi:10.1080101431168708948613.
- Wu, H., and Li, Z.-L 2009. Scale issues in remote sensing: a review on analysis, processing and modeling. Sensors, 9: 1768. doi:10.33901 s90301768. PMID•. 22573986.